Particle filter based volcanic ash emission inversion applied to a hypothetical sub-Plinian Eyjafjallajökull eruption using the chemical component of the Ensemble for Stochastic Integration of Atmospheric Simulations (ESIAS-chem) version 1.0

Philipp Franke[1,2], Anne Caroline Lange[1,2], and Hendrik Elbern[1,2]

[1]Institute of Energy and Climate Research: Troposphere (IEK-8), Forschungszentrum Jülich GmbH, 52425 Jülich, Germany
[2]Rhenish Institute for Environmental Research at the University of Cologne, Aachener Str. 209, 50931 Köln, Germany

Correspondence: Philipp Franke (p.franke@fz-juelich.de)

Abstract. A particle filter based inversion system to derive time- and altitude-resolved volcanic ash emission fluxes along with its uncertainty is presented. For the underlying observation information only vertically integrated ash load data as provided by retrievals from nadir looking imagers mounted on geostationary satellites is assimilated. We aim to estimate the temporally varying emission profile with error margins, along with evidence of its dependencies on wind driven transport patterns

5   within variable observation intervals. Thus, a variety of observation types, although not directly related to volcanic ash, can be utilized to constrain the probabilistic volcanic ash estimate. The system validation addresses the special challenge of ash cloud height analyses in case of observations restricted to bulk column mass loading information, mimicking the typical case of geostationary satellite data. The underlying method rests on a linear-combination of height-time emission finite elements of arbitrary resolution, each of which is assigned to a model run subject to ensemble-based space-time data assimilation. Employ-

10   ing a modular concept, this setup builds the Ensemble for Stochastic Integration of Atmospheric Simulations (ESIAS-chem) that comprises a particle smoother in combination with a discrete-grid ensemble extension of the Nelder-Mead minimization method. The ensemble version of the EURopean Air pollution Dispersion - Inverse Model (EURAD-IM) is integrated into ESIAS-chem but can be replaced by other models. The performance of ESIAS-chem is tested by identical twin experiments. The application of the inversion system to two notional sub-Plinian eruptions of the Eyjafjallajökull with strong ash emission

15   changes with time and injection heights demonstrate the ability of ESIAS-chem to retrieve the volcanic ash emission fluxes from the assimilation of column mass loading data only. However, the analysed emission profiles strongly differ in their levels of accuracy depending of the strength of wind shear conditions. Under strong wind shear conditions at the volcano the temporal and vertical varying volcanic emissions are analyzed up to an error of only 10 % for the estimated emission fluxes. For weak wind shear conditions, however, analysis errors are larger and ESIAS-chem is less able to determine the ash emission flux

20   variations. This situation, however, can be remedied by extending the assimilation window. In the performed test cases, the ensemble predicts the location of high volcanic ash column mass loading in the atmosphere with a very high probability of >95 %. Additionally, the ensemble is able to provide a vertically resolved probability map of high volcanic ash concentrations to a high accuracy for both, high and weak wind shear conditions.

1 Introduction

Apart from water and carbon dioxide, volcanic eruptions release enormous amounts of harmful trace gases and particulate
matter. Chemistry transport models have limits in estimating the emission strength of those events in an accurate temporal
and spatial resolution because the emission characteristics, i. e. the emission strength and its temporal and vertical distribution
within the eruption plume, are typically not well known (e. g., Bursik et al., 2012). Therefore, special assessment methods for
unexpected emission events are necessary. Because of the potential threat to human health, economy, and climate of volcanic
eruptions, a detailed knowledge not only about the spatial and temporal variations of the emissions and its strength is required
but also accurate information about the analysis error.

Typically, volcanic eruptions occur as sequences of emissions with highly varying ejection mass and height. Only limited ob-
servations of volcanic ash emission parameters are available (e.g. eruption plume heights retrieved form radar measurements,
Arason et al. (2011)). Thus, eruption models are applied to simulate volcanic emissions instead. These may be inferred from
statistical data (e. g., Sparks et al., 1997; Mastin et al., 2009) or physical processes (e. g., Woodhouse et al., 2013; Folch et al.,
2016). Statistical models are based on observational data from only a few, highly heterogeneous volcanic eruptions, while
physical plume-scale models require vent and magma details, which are poorly known, and thus making these models highly
uncertain.

Another potential way to constrain volcanic ash emissions is the use of observations of volcanic ash in the atmosphere. Ad-
vanced numerical analysis techniques for quantitative and stochastic estimation of volcanic ash concentrations and emissions
use mostly satellite observations of column mass loading via data assimilation methods (e. g., Wilkins et al., 2016a). In con-
trast to lidar observations, e. g. from the Cloud Aerosol LIdar with Orthogonal Polarization (CALIOP) instrument on board
CALIPSO satellite (Winker et al., 2009) or the ground (e. g. via the European Aerosol Research Lidar Network, EARLINET[1]),
column mass loading observations do not provide any information about the vertical distribution of volcanic ash. Therefore,
multiple data assimilation methods make assumptions about the vertical extent of the volcanic ash cloud (e. g., Schmehl et al.,
2012; Wilkins et al., 2016b; Zidikheri et al., 2016). In addition to column mass loading observations of volcanic ash clouds,
Zidikheri et al. (2017a) suggested to use brightness temperature measurements to distinguish regions with high mass load from
those with low mass load. The great advantage of using column mass loading observations as available from, for example, the
Spinning Enhanced Visual and InfraRed Imager (SEVIRI) on board Meteosat Second Generation (Schmetz et al., 2002) is the
horizontally more complete picture of the volcanic ash extent. Observations of column mass loading and lidar measurements
are restricted to areas without water cloud cover. Finally, the challenge of estimating the three-dimensional volcanic ash field
from two-dimensional volcanic ash column mass loading observations remains to be solved.

First estimations of volcanic ash emissions from the 2010 Eyjafjallajokull eruption in a high temporal and vertical resolution
were made by Stohl et al. (2011) and later by Kristiansen et al. (2012) and Kristiansen et al. (2015). Their algorithm bases on
the inversion technique of Eckhardt et al. (2008), in which an optimal combination of distinct emission packages is estimated
using a least squares method. Further developments of assimilation systems for volcanic ash emissions include the "genetic

---

[1]https://www.earlinet.org/index.php?id=earlinet_homepage

algorithm variational approach" (Schmehl et al., 2012) and an adjoint free ensemble version of the 4d-var data assimilation method (Lu et al., 2016).

Zidikheri et al. (2016) and later Zidikheri et al. (2017b) developed an assimilation system that aims to analyze the horizon-
60 tal distribution of volcanic ash column mass loading rather than the emission strength. This was extended by Zidikheri et al. (2017a) to additionally estimate the height and the particle size distribution of volcanic ash emissions using a parameter re-finement method. Wilkins et al. (2014) used the "data insertion" method in which observed volcanic ash column mass loading act as virtual sources for volcanic ash with a predefined vertical distribution. The algorithm was successfully applied to the eruptions of Eyjafjallajökull, Iceland, 2010 (Wilkins et al., 2016b) and Grímsvötn, Iceland, 2011 (Wilkins et al., 2016c).

65 A general framework for calculating uncertainties of volcanic ash concentrations for constant volcanic ash emissions given "any model and any observational data" was proposed by Denlinger et al. (2012). Bursik et al. (2012) applied the "polynomial chaos quadrature weighted estimate" (PCQWE) method to volcanic ash emissions. This approach was further extended by Stefanescu et al. (2014) to take uncertainties in the wind fields into account as well. An extension of the polynomial chaos quadrature method was proposed by Madankan et al. (2014) to generate hazard maps of volcanic ash in the atmosphere. The
70 PCQWE method aims to map uncertainties in the input parameters of a volcanic eruption onto the volcanic ash concentrations without accounting for constraining volcanic ash observations. Additionally, Dare et al. (2016) investigated the influence of meteorological ensemble forecasts on the dispersion of volcanic ash. They found that not only the ensemble statistics should be evaluated but also may the single ensemble members contribute significant information to the distribution of volcanic ash.

Although these studies applied highly advanced data assimilation methods for analyzing the emission strength and its uncer-
75 tainty, a joint assessment of both, emission strength and its uncertainty, in a high temporal and vertical resolution has not yet been evaluated. Thus, this contribution aims to fill this gap by providing such estimates of emission strength and its uncertainty in a high temporal and spatial resolution resulting in height-resolved probability maps of volcanic ash concentrations.

Section 2 describes the full stochastic assimilation system ESIAS-chem and the methods applied. The potential and limita-tions of ESIAS-chem are shown by identical twin experiments in section 3 for predictions of the ensemble mean volcanic ash
80 concentration and the posterior probability of high volcanic ash content. Conclusions will be given in section 4.

2 Ensemble for Stochastic Integration of Atmospheric Simulations (ESIAS)

The Ensemble for Stochastic Integration of Atmospheric Simulations (ESIAS) is designed to control simultaneous and inter-active runs of ultra-large ensembles of complex atmospheric models, with special dedication to numerical weather prediction models and chemistry transport models, along with extensions to include data assimilation modules. There exist a meteoro-
85 logical (ESIAS-met) and an atmospheric chemical part (ESIAS-chem). The emphasis of this paper is placed on the latter for probabilistic atmospheric chemistry-transport-diffusion simulations with data assimilation. In the following, the main com-ponents of the ESIAS-chem system are introduced, which include an ensemble of emission packages, a modified version of the Nelder-Mead minimization algorithm, and a particle filter and resampling algorithm. Finally, the full stochastic particle smoother algorithm of ESIAS-chem for probabilistic volcanic ash analyses is described.

2.1 Ensemble of emission packages

The main assignment of ESIAS-chem is to simulate normalized emissions as a set of N_{emis} pairwise distinct emission packages (emission scenarios in the terminology of Stohl et al. (2011)) each of which with a unit mass of ash. More specific, the eruption plume is discretized into N_T time steps and K_{max} vertical layers. Emission strength and plume height of a volcanic eruption may vary quickly, which may result in multiple maxima in the vertical distribution of the volcanic ash emissions within the discretized emission profile. This is accounted for in our approach. Each ensemble member simulates the volcanic ash concentration released by a single emission package for an individual time step and height interval. A similar approach for estimating the volcanic ash column mass loading was used by Stohl et al. (2011) and Kristiansen et al. (2015) aiming to estimate the optimal emission profile but not its uncertainty.

The optimal combination of the emission packages is calculated by minimizing the cost function $J(\mathbf{a})$

$$\hat{\mathbf{a}} = \text{argmin}\,(J(\mathbf{a})) = \text{argmin}\left(\sum_{i=1}^{N_{emis}}(HM[a_i\mathbf{s}_i] - \mathbf{y})^T\mathbf{R}^{-1}(HM[a_i\mathbf{s}_i] - \mathbf{y})\right),\tag{1}$$

with the source-receptor model M mapping the unique emissions $\mathbf{s}_i$ of ensemble member i onto the model state. Herein, $\mathbf{s}_i = (0,\ldots,0,c,0,\ldots,0)^T = c * \mathbf{e}_i$ is a $K_{max} * N_t = N_{emis}$ dimensional vector with $c = const$ the default mass of ash in the emission package and $\mathbf{e}_i$ the ith unit vector. Scalar a_i is the scaling factor for the ith emission package. For the optimization, a_i values are packed into vector $\mathbf{a}$ resulting in optimal values $\hat{\mathbf{a}}$. Further, $\mathbf{R}$ is the observation error covariance matrix and H denotes the observation operator for volcanic ash column mass loading, which is given by

$$\hat{x} = 10^6\sum_{k=1}^{K_{max}} x_k\Delta z_k,\tag{2}$$

where x_k is the modeled concentration of volcanic ash, given in [μgm^{-3}] and Δz_k is the thickness of model layer z in [m]. It is noticed that the vertical and temporal resolution of the emissions can be varied by changing the parameters K_{max} and N_t, thus, making them independent from the vertical and temporal resolution of the model. Although the algorithm is designed for column mass loading observations, it is as well applicable to observations of any volcanic ash related quantity, e. g. brightness temperature as proposed by Zidikheri et al. (2017a).

2.2 Nelder-Mead algorithm

The minimization problem posed by (1) is solved using the Nelder-Mead algorithm (Nelder and Mead, 1965). The Nelder-Mead minimization algorithm is proved to be robust, especially in cases where the function to be minimized has discontinuities or the function values are noisy (see McKinnon, 1998), which is expected to be likely in highly variable volcanic eruptions. Additionally, the Nelder-Mead algorithm needs relatively few function evaluations (mostly 1-2 per iteration, Lagarias et al., 1998).

The idea of the algorithm is to move a simplex on the surface of the cost function to find its minimum in a N-dimensional space. The version of the Nelder-Mead method used in this study follows Gao and Han (2012) and utilizes adaptive parameters

120   controlling the step size for each iteration of the minimization. The version has been implemented for parallel operation (Klein
and Neira, 2014; Lee and Wiswall, 2007).

The minimization was performed in $\mathbb{N}_0^N$, which has been found to be more effective than the minimization in $\mathbb{R}^N$. Thus, only integer values are accepted for the scaling factors a_i of the emission packages. By applying this constraint it is assumed that the introduced errors are of lower order than the error introduced by the temporal resolution of the emission packages. Further, in

125   order to generate an ensemble of analyses and because the minimization depends on the initial simplex, the minimization tasks are performed for each ensemble member with different initial simplices. Thus, the minimization algorithm is called hereafter discrete-grid ensemble Nelder-Mead method (DENM).

2.3 Particle filter

The particle filter methodology, also known as sequential importance resampling, is used as a non-Gaussian data assimilation
130   method for large ensemble simulations. The particle filter method was proposed by Gordon et al. (1993) and further popularized in oceanography and meteorology by van Leeuwen (2009). It develops from Bayes' Theorem

$$p(\mathbf{x}|\mathbf{y}) = \frac{p(\mathbf{y}|\mathbf{x})p(\mathbf{x})}{\int p(\mathbf{y}|\mathbf{x})p(\mathbf{x})d\mathbf{x}}, \tag{3}$$

where p($\cdot$) denotes the probability density function (PDF), $\mathbf{y}$ the observations, and $\mathbf{x}$ the model state. The a priori PDF is approximated by an ensemble of N_{ens} model runs

135   $$p(\mathbf{x}) = \frac{1}{N_{ens}} \sum_{i=1}^{N_{ens}} \delta(\mathbf{x} - \mathbf{x}_i), \tag{4}$$

where $\delta(\cdot)$ denotes the Kronecker delta function and $\mathbf{x}_i$ is the model state of particle (ensemble member) i.

Applying (4) results in

$$p(\mathbf{x}|\mathbf{y}) = \sum_{i=1}^{N_{ens}} \frac{p(\mathbf{y}|\mathbf{x}_i)}{\sum_{j=1}^{N_{ens}} p(\mathbf{y}|\mathbf{x}_j)} \delta(\mathbf{x} - \mathbf{x}_i) = \sum_{i=1}^{N_{ens}} w_i \delta(\mathbf{x} - \mathbf{x}_i), \tag{5}$$

where an individual weight w_i is applied to each ensemble member. Thus, each ensemble member is weighted by the normal-
140   ized likelihood of its current model state. It is noted that in the particle filter method no assumptions of the error statistics of the model state and the observations were made. Further, the particle filter method is directly applicable to nonlinear models. In particle filters, filter degeneracy often occurs (cf. Bengtsson et al., 2008; Snyder et al., 2008; Bickel et al., 2008), especially in high dimensional problems. Several methods exist to reduce filter degeneracy (see e.g. van Leeuwen (2009) for a review) and the reader is referred to the original papers for more information. In this model setup for improving the ensemble skill, residual
145   resampling (Liu and Chen, 1998) is used, in which the ensemble members with high weights are duplicated and perturbed, replacing ensemble members with vanishing weights. Thus, the statistical meaning of the ensemble is preserved.

2.4 ESIAS-chem

ESIAS-chem is designed as a flexible analysis system for quantitative volcanic ash assessments, along with a quantification of the uncertainty of the optimal emission flux profile. Further, it is applicable to other accidentally released matter and con-
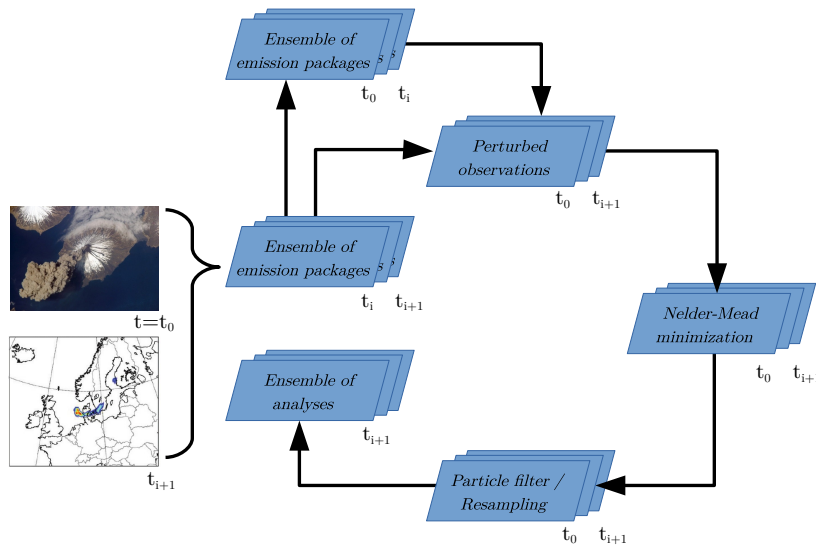
Figure 1. Schematic of the ESIAS-chem analysis workflow. The analysis is initiated at time $t = t_0$ and restarted, when new observations become available. Here, t_{i+1} corresponds to the observation time. Credits for volcano image: NASA (https://www.nasa.gov/multimedia/imagegallery/image_feature_756.html; Cleveland volcano, Aleutian Islands, latest access: 13 January, 2021).

150   stituents, suitably constraining observations are available. In order to account for meteorological uncertainties, ESIAS-chem is capable to be coupled with ensembles of meteorological fields. The workflow of the system is illustrated in Fig. 1. Once a volcanic eruption is detected ($t = t_0$), the system is started by generating the ensemble of emission packages (cf. section 2.1) of default mass of volcanic ash.

As long as no observations are available, this ensemble serves as an estimation predictor of the maximum possible volcanic
155   ash extension without providing quantitative volcanic ash estimates. Once new observations become available, the system is restarted at time $t = t_0$. The previously calculated ensemble of emission packages is reused, now integrated forward in time until the observation time ($t = t_{i+1}$). Further ensemble members are included to account for the latest emissions in the interval $[t_i, t_{i+1}]$.

The ensemble is compared with the observations to calculate (1), which is to be minimized using the DENM method. As this
160   algorithm is optimized for the estimation of column integrated ash loading in a considerably underdetermined control system, a regularization term is added to the cost function (1), leading to

$$J(\mathbf{a}) = \mathbf{a}^T \mathbf{B}^{-1} \mathbf{a} + \sum_{i=1}^{N_{emis}} (HM[a_i \mathbf{s}_i] - \mathbf{y})^T \mathbf{R}^{-1} (HM[a_i \mathbf{s}_i] - \mathbf{y}). \tag{6}$$

This choice restricts the scaling factors **a** to vary too strongly. As each volcanic eruption has its own individual emission characteristics, no fixed assumptions have been made for matrix **B**, which accounts for correlations of the individual emission packages. Those emission characteristics may be (partial) eruption column collapse, abrupt change in emission strength, or multiple vents within one model grid box erupting in different strength and height. Here, **B** is chosen as diagonal matrix $\mathbf{B} = diag(10)$ but other choices may also be possible. This value for **B** was found to be optimal for this study by several tests. The minimization is performed with an ensemble of arbitrarily varying initial simplices

$$\mathbf{a}_0 = \{a_{10}, a_{20}, \ldots, a_{i0}, \ldots, a_{N_{emis}-10}, a_{N_{emis}0}\}.$$

Thus, the regularization term was chosen in order to maintain a suitable spread of the analysis ensemble. To account for common eruption column profiles, it has been further tested to start the minimization with an ensemble of predefined umbrella-shaped emission profiles of different emission strength and temporal and vertical distributions (not shown). At least for the current study it has been found that the analysis using these predefined emission profiles performed worse than using arbitrary emission profiles, mainly because in the former case the minimization was too strongly restricted by the predefined emission profile shape and suppressed variations in the emission profile. Thus, the current analysis is performed using an arbitrary set of initial emission profiles. In addition, the observation errors are represented by perturbed observations (cf. Houtekamer and Mitchell, 1998), which are assimilated by ESIAS-chem leading to larger ensemble spreads.

Finally, a particle filter step is applied. The weights, which result from the filtering step, are applied to the optimized emission profiles. If new observations become available the assimilation window may be elongated to use the new observations for updating the emissions within the whole assimilation window $[t_0, t_{i+1}]$.

3   Identical twin experiments

The utility of the system to provide quantitative estimates of the volcanic ash emission uncertainty is explored by identical twin experiments. Identical twin experiments are necessary, yet not sufficient standard test procedures for validating spatio-temporal data assimilation and inverse modelling set-ups. They rest on the "perfect model assumption" and its analog for the data side: exactly known accuracy and representativity. This provides a total knowledge of the "synthetic truths" as given by simulations with the same model and extraction of artificial "measurements/soundings" thereof. Given the identical twin assumption the experiment is then to be made realistic in all other respects, as the two different weather conditions on our case. Daley (1991) concludes however, that identical twin experiments "err on the optimistic side" (loc. cit.). Yet, the applicability of ESIAS-chem to real volcanic eruptions will be shown in a companion paper. In this study, ESIAS-chem is coupled to the regional air quality model EURAD-IM (EURopean Air pollution Dispersion - Inverse model, Elbern et al., 2007). The simulations have been run on the JUQUEEN supercomputer (Jülich Supercomputing Centre, 2015). EURAD-IM comes with the adjoint code of the chemical and aerosol modules for four–dimensional variational data assimilation. Nested analyses with up to 1 km resolution are possible while coupled with ESIAS-chem (not applied in this analysis).

To investigate the potential and limitations of the proposed assimilation system ESIAS-chem for volcanic ash emission assessments, column mass loading of volcanic ash in $[\mathrm{gm}^{-2}]$ is extracted as fictional observation data y_i every 6 hours from a

'nature' run, simulated by the forward model of EURAD-IM for 15 April and 29 April 2010, which were chosen as differing meteorological setting with strong and weak wind conditions above the North-Atlantic, respectively. These data mimic cloud free retrievals from the Spin Enhanced Visible and Infrared Imager (SEVIRI) onboard the geostationary Meteosat Second Generation satellite, with significantly larger time steps (six hours in this analysis), however. This renders the observation operator

200 to be the identity matrix. The synthetic observations from the nature run are extracted from the full domain including grid cells containing volcanic ash and those without volcanic ash. The information of ash free areas is necessary in order to avoid estimates of spurious emissions at false times and heights in the analysis.

The uncertainty of volcanic ash column mass loading observations is about 40 % (Kristiansen et al., 2015, and references therein). As it was decided to assimilate all synthetic observations regardless of their value, a special treatment for observed

205 low values at the edge of the volcanic ash clouds is needed, which can be accomplished by altering the observation error. As the mismatch between the model and observations in (1) is scaled by the observation error covariance matrix, a relative error of low volcanic ash values overemphasizes the system to these observations of low volcanic ash content. Further, no relative error for observations of no-volcanic ash observations can be obtained. Therefore, it was decided to use the following expression for the observation error σ_{y_i} with a minimum error of $0.1 \ \mathrm{gm}^{-2}$

210 $$\sigma_{y_i} = \max \left[\frac{(y_i * 0.4)^2}{\max_j(y_j * 0.4)}, 0.1 \right]. \tag{7}$$

With this choice of observation error, the impact of low volcanic ash values observed at the edge of the volcanic ash cloud on the analysis is diminished.
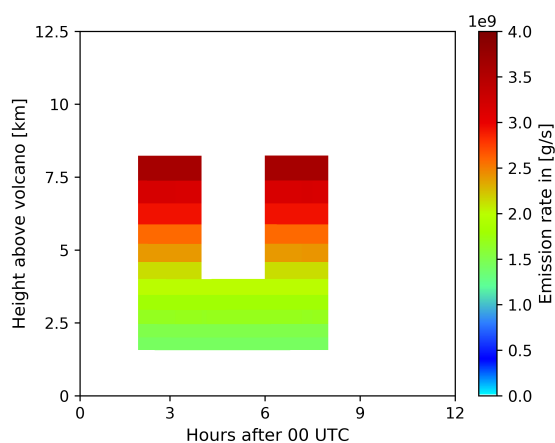
Figure 2. Hovmoeller-like plot of the nature run emission profile for the performance analysis of ESIAS-chem in dependence on the length of the assimilation window on 15 April and 29 April 2010. Shown is the emission rate (colored) for a given time (x-axis) and height above the volcano (y-axis).

The performance of ESIAS-chem for different assimilation window lengths is tested for a hypothetical eruption of the Icelandic volcano Eyjafjallajökull under different, yet real meteorological conditions. The Hovmoeller-like plot of the nature run emission profile is shown in Fig. 2. It shows the variable emission rate by a height-time graphic above the volcano. The selected sub-Plinian eruption type (Bardintzeff and McBirney, 2000) is characterized by two short explosive phases between 02-04 UTC and 06-08 UTC reaching a height of approx. 8 km above the volcano.

The length of the assimilation window influences the performance of the data assimilation algorithm due to the influence of vertical and horizontal mixing and vertical wind shear. Hence, the performance of ESIAS-chem is tested for different assimilation window lengths. All assimilation windows start at 00 UTC for the specific day and last for 06-36 hours. Fig. 3 illustrates the different assimilation window lengths. The assimilation windows differ in length by multiples of 06 hours. Certainly, by increasing the assimilation window length the observations include more information, as the residence time of volcanic ash in the atmosphere is increased. Contrary, vertical and horizontal mixing of volcanic ash emitted may limit the benefit that is gained by increasing the assimilation window length. Once the volcanic ash emissions are optimized, a forecast is appended until 36 hours after the simulation start (hatched areas in Fig. 3). Thus, beneficial impacts of the assimilation results for the analyses with differing assimilation window lengths can be assessed.

The first real weather test day to which ESIAS-chem is applied is 15 April 2010, which was characterized by strong west–north–westerly winds at Iceland. This is illustrated by the wind profile at the volcano (Fig. 4a) for the whole simulation length of 36 hours and the wind field over Europe at approx. 5 km height on 15 April 2010, 12 UTC (Fig. 4b). During this day, the polar front and the polar jet stream are located above Iceland, driving the volcanic ash to travel fast southeast towards continental Europe, with wind speeds of up to 60 ms^{-1} at heights of 5–8 km. Fig. 4c shows a vertical cross section of pressure and temperature along the red line in Fig. 4b at 12 UTC on 15 April 2010. As indicated by the intersection of the isobars and isotherms, 15 April 2010 is characterized by substantial vertical wind shear above Iceland, which is expected to ease the
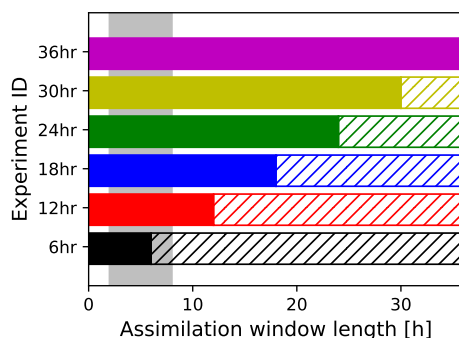
Figure 3. Illustration of the varying assimilation window lengths for the identical twin experiment (filled bars). After each assimilation window, a free forecast until 36 hours after the start of the simulation is appended (hatched bars). Color codes and experiment IDs correspond to the annotations in the subsequent figures. The gray area indicates the duration of the volcanic eruption.

distinction of volcanic ash emitted at different heights as seen from above.

235   In addition to the synoptic scenario on 15 April 2010 a second analysis of ESIAS-chem's performance is made for a hypo-
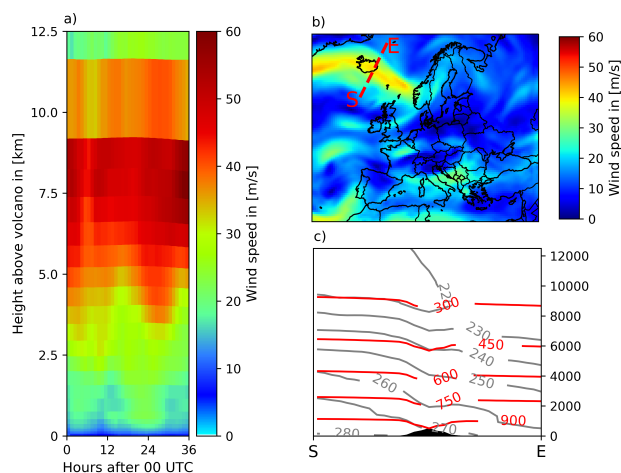
Figure 4. Meteorological conditions on 15 April 2010. (a) Wind speed above the volcano for the whole simulation period. (b) Wind speed in approx. 5 km height on 15 April 2010, 12 UTC. (c) Vertical cross-section of isobars (red) and isotherms (grey) along the red line in b) on 15 April 2010, 12 UTC.
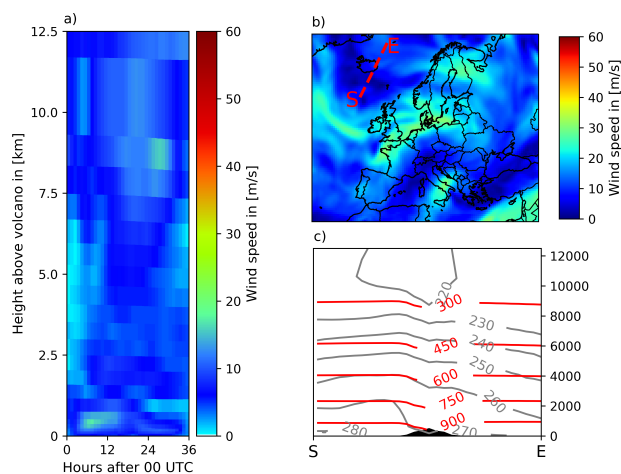
Figure 5. Meteorological conditions on 29 April 2010. (a) Wind speed above the volcano for the whole simulation period. (b) Wind speed in approx. 5 km height on 29 April 2010, 12 UTC. (c) Vertical cross-section of isobars (red) and isotherms (grey) along the red line in b) on 29 April 2010, 12 UTC.

thetical sub-Plinian eruption of the Eyjafjallajökull volcano on 29 April 2010 (Fig. 5). The same emission profile is taken as depicted in Fig. 2. This day is characterized by weak winds of approximately $10\,\mathrm{ms}^{-1}$ in the vicinity of the volcano, which is illustrated by Fig. 5. Thus, the emitted volcanic ash is only slowly transported. Additionally, the vertical wind shear on 29 April 2010, 12 UTC, is low, as indicated by a higher barotropicity above Iceland (Fig. 5c). The two dates were chosen because of

240   their different wind patterns and the real eruption of the Eyjafjallajökull that occurred during these days. Hence, the identical twin experiment provides an optimal case scenario for the application of ESIAS-chem to real volcanic eruptions.

In order to validate the results of the stochastic assimilation method, first the volcanic ash cloud of the ensemble mean is compared to the nature run. Two measures are considered, which provide information about the accuracy of the horizontal extent of the volcanic ash cloud and the distribution of volcanic ash within the cloud. The former is investigated by the pattern

245   correlation coefficient (pcc, cf. Zidikheri et al., 2016) of the column mass loading of the nature run and the ensemble mean. The latter is analyzed by the relative mean absolute error (RMAE) of the column mass loading.

The pcc is defined by (Zidikheri et al. (2016))

$$pcc = \frac{<\mathbf{va}'_x, \mathbf{va}'_y>}{|\mathbf{va}'_x||\mathbf{va}'_y|}, \tag{8}$$

with $\mathbf{va}' = \mathbf{va} - \overline{\mathbf{va}}$. Herein, the entries of the volcanic ash detection vector $\mathbf{va}$ for the model mean (subscript x) and observa-

250   tions (y) are equal to 1 if the grid column contains volcanic ash above $0.2\,\mathrm{gm}^{-2}$, which is the detection limit of volcanic ash column mass loading observations (Prata and Prata, 2012), and 0 otherwise. The mean volcanic ash detection $\overline{\mathbf{va}}$ is calculated by

$$\overline{\mathbf{va}} = <\mathbf{1}, \mathbf{va}> / <\mathbf{1}, \mathbf{1}>, \tag{9}$$

where $\mathbf{1}$ denotes the vector with 1 on all entries and $<\cdot, \cdot>$ indicates the scalar product. The pattern correlation coefficient gives

255   information about the compliance between the simulated and observed horizontal distribution of volcanic ash in the atmosphere. If the volcanic ash clouds, indicated by the column mass loading, of the nature run and the ensemble mean perfectly coincide, the pattern correlation coefficient equals 1. If the volcanic ash clouds of the nature run and the ensemble mean are totally disjoint, the pattern correlation coefficient equals 0. It is noted that for this model setup with perfect meteorology, pcc < 1 indicates that the analysis contains volcanic ash either in model layers or at times, where no volcanic ash is emitted in the

260   nature run.

The RMAE is defined by

$$RMAE = 100\frac{1}{N_y}\sum_{j=1}^{N_y}\left|\frac{\overline{x}_j - y_j}{y_j}\right|, \tag{10}$$

where N_y is the number of grid columns in which volcanic ash column mass loading of the nature run y_j and the ensemble mean $\overline{x}_j$ are $\geq 0.2\,\mathrm{gm}^{-2}$. The RMAE is as well calculated for volcanic ash concentrations, for which this threshold is

265    $\geq 10\,\mathrm{\mu gm}^{-3}$. In this case, y_j corresponds to the volcanic ash concentration simulated by the nature run. The RMAE measures the relative difference of column ash mass loads (or volcanic ash concentrations) between nature run and ensemble mean,

averaged over all grid cells. Higher values of the RMAE are a result of different height–time–mass emission patterns between the nature run and the ensemble mean, given the assumed perfect meteorology used in this analysis.

The pattern correlation coefficient is shown in Fig. 6 for the two analysis days. The lines in Fig. 6 indicate results for differ-

270   ent assimilation window lengths as illustrated by Fig. 3. Fig. 6 shows a constantly large pattern correlation coefficient > 0.95 after the artificial eruption terminated at 08 UTC for both analysis days, except for assimilation window lengths of 06 and 12 hours. By applying an assimilation window of 06 hours from the simulation start, the artificial volcanic eruption has not terminated, thus, the latest emissions from the nature run volcanic eruption are not considered in the analysis. This leads to a reduced pcc for the 06 hour assimilation window test case. The assimilation window of 12 hours ends four hours after the

275   termination of the artificial volcanic eruption. The reduced pcc exhibits that this short assimilation window is not sufficient in order to analyze the correct emission profile. Thus, with increasing time after the end of the assimilation window, the pcc decreases to approx. 0.88 on 15 April 2010 and approx. 0.92 on 29 April 2010. The high pcc values indicate that the assimilation of column mass loading to estimate volcanic ash emissions succeeds to retrieve the horizontal extent of the volcanic ash cloud. Again, the pattern correlation coefficient does not account for deviations in the strength of volcanic ash column mass loading

280   at locations in which the ensemble mean and the nature run differ in volcanic ash load.

Increasing the assimilation window length (i.e. taking later observations into account) increases the pattern correlation coefficient on both days. The analysis suggests that for the respective test cases an assimilation window of 18 hours, that is 10 hours after the artificial eruption terminated, is sufficient for ESIAS-chem to analyze the exact location of the volcanic ash cloud as observed from space leading to a pcc value that remains high (> 0.95) throughout the full analysis time period of 36 hours.

285   Fig. 6 demonstrates that the assimilation system is able to accurately analyze the horizontal extend of the volcanic ash cloud.

Fig. 7 shows the RMAE for volcanic ash column mass loading on both days. The RMAE is relatively constant for the duration of the simulations, except for the 12 h assimilation window case in Fig. 7a. At the end of the simulation time at 36 hours, the
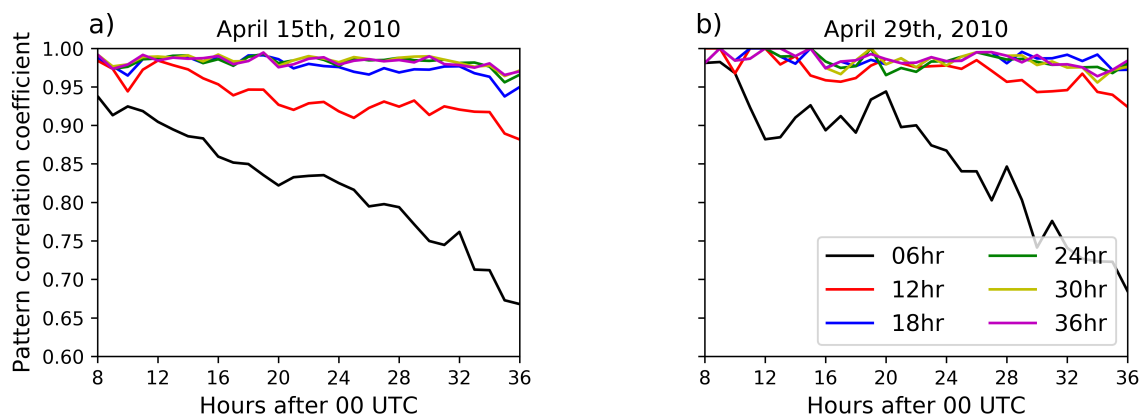
Figure 6. Pattern correlation coefficient defined by (8) for the eruption on (a) 15 April 2010 and on (b) 29 April 2010. The different lines indicate different assimilation window lengths from 06 hours (gray) to 36 hours (magenta) as defined by Fig. 3.
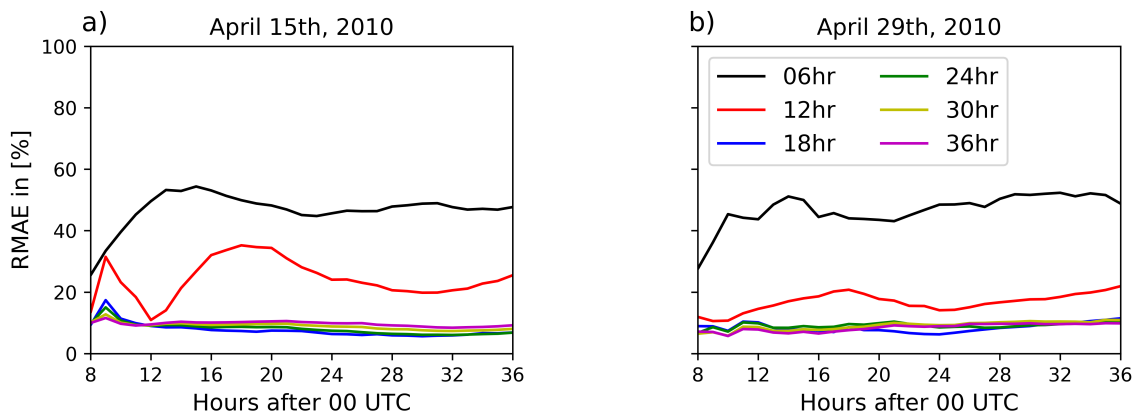
Figure 7. Relative mean absolute error of column mass loading defined by (10) for the eruption on (a) 15 April 2010 and on (b) 29 April 2010. The different lines indicate different assimilation window lengths from 06 hours (gray) to 36 hours (magenta) as defined by Fig. 3.

test cases with longer assimilation windows ($\geq$ 18 hours) show a RMAE of the order of 10 % for both days. These low values show the good performance of the analysis for these assimilation window lengths with respect to the nature run. In principle,

290 Fig. 7 corroborates the same findings that are analyzed for the pattern correlation coefficient, i. e. increasing the assimilation window length decreases the error of the ensemble mean. For both days and meteorological circulation patterns, an assimilation window of 18 hours is sufficient to reduce the RMAE to a value of approx. 10 % for column mass loading values above 0.2 gm^{-2}. On 15 April 2010 assimilation windows larger than 24 hours result in a slightly higher RMAE than the analysis using an assimilation window of 18 hours. This is a result of the convergence of volcanic ash in the upper troposphere south

295 of Norway around 24 hours after the simulation has started (not shown). Thus, additional observations at later times do not contribute significant information to the assimilation system. In summary, Fig. 7 proves that the assimilation system is able to analyze the distribution of volcanic ash column mass loading properly for weak and strong wind conditions.

The above analysis focuses on the comparison of the nature run and the ensemble mean with respect to column mass loading of volcanic ash. Thus, it does not provide any information about the vertical distribution of volcanic ash. The ability of ESIAS-

300 chem to infer vertical profiles of volcanic ash is given in Fig. 8, which displays the relative mean absolute error of the volcanic ash concentrations above 10 $\mu\mathrm{gm}^{-3}$. The RMAE of the volcanic ash concentrations decreases by increasing the assimilation window length, which is especially visible for 29 April 2010. On both days, an assimilation window of only 6 hours results in a RMAE larger than 100 %. Therefore, this test case is not shown in Fig. 8. On average, the RMAE reduces to about 20 % on both days for assimilation windows larger than 18 hours, which shows the good performance of the ESIAS-chem analysis not

305 only in terms of column mass loading but also in terms of the vertical distribution of the volcanic ash in the atmosphere.

The analysis results using an assimilation window of 24 hours are investigated exemplary in more detail. This test case is chosen as the previous analysis showed the good performance of the 24 hour assimilation window experiments. Further, an assimilation window of 24 hours is a reasonable choice for either analysis of longer lasting volcanic eruptions or an operational

use. Fig. 9 and Fig. 10 display the profile of (a) the nature run emissions, (b) the ensemble mean emissions, (c) the relative

310   error of the ensemble mean

$$RE = \frac{\overline{x} - y}{max(\overline{x})}, \tag{11}$$

and (d) the relative ensemble standard deviation

$$\sigma_{rel} = \frac{\sigma_x}{max(\overline{x})}, \tag{12}$$

for the 24 hour assimilation window experiments on 15 April and 29 April 2010. Herein, $\overline{x}$ and y are the ensemble mean and

315   nature run emissions, respectively, and σ_x is the ensemble standard deviation.

The total nature run emissions on both days ($4.25 \cdot 10^8$ tons and $4.30 \cdot 10^8$ tons on 15 April and 29 April, respectively) are

well captured by the analyzed total emissions with mean emissions of $4.58 \cdot 10^8$ tons and $4.10 \cdot 10^8$ tons, respectively, and

standard deviations of $3.67 \cdot 10^7$ tons and $3.47 \cdot 10^7$ tons. The relative error of the total emitted volcanic ash is 7.7 % and

4.7 %, respectively. On 15 April 2010, the analyzed emission profile of the ensemble mean shows the two explosive eruptions

320   of the nature run emission profile with the correct height of the maximum emissions at the right time (Fig. 9b). Even though the

ensemble mean shows a vertically and temporally smoothed emission profile, the false emissions are low with respect to the

maximum emissions. The relative error of the ensemble mean emissions is of the order of 10 %–20 % for most emission times

and heights (cf. Fig. 9c) and therefore, the results are similar to the analysis presented before. The relative ensemble standard

deviation is of the same order as the relative error of the ensemble mean emissions, indicating a reasonable ensemble spread.

325   The analyzed emission profile of the ensemble mean on 29 April 2010 (Fig. 10b) however shows strong deviations from the

nature run emission profile (Fig. 10a). Although the highest level emissions of the nature run emission profile in 8 km height
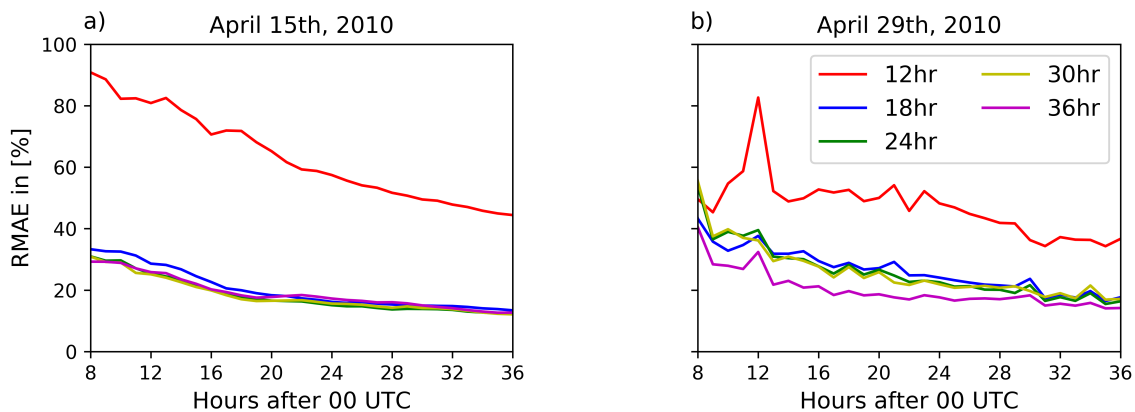
Figure 8. Relative mean absolute error of the volcanic ash concentrations defined by (10) for the eruption on (a) 15 April 2010 and on (b) 29 April 2010. The different lines indicate different assimilation window lengths from 12 hours (red) to 36 hours (magenta) as defined by Fig. 3.
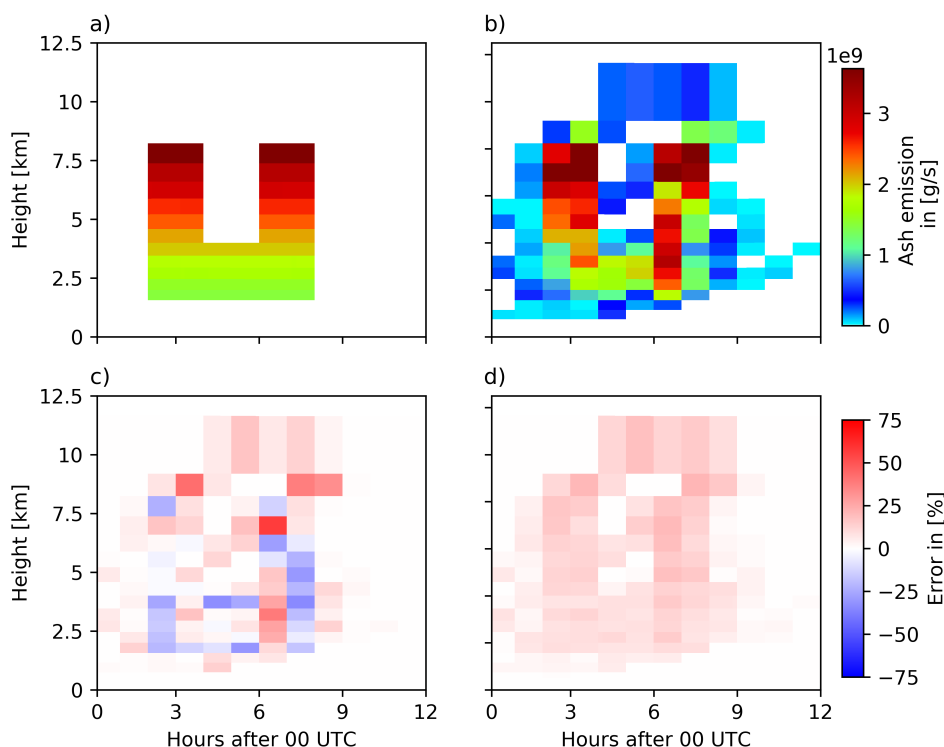
Figure 9. Comparison of the emission profiles of the nature run and ensemble mean for 15 April 2010. The figure shows (a) the nature run emission profile and (b) the ensemble mean emission profile. For comparison, (c) the relative error of the ensemble mean and (d) the relative ensemble standard deviation are illustrated.

are well captured by the ensemble mean, at lower levels no distinction between the two explosive eruptions is obtained. In comparison to the analyzed emissions on 15 April 2010, on 29 April 2010 the analyzed emissions of the ensemble mean are more uniform in time and height. Thus, large errors in both directions can be identified: negative errors during the explosive

330 eruptions at around 03 UTC and 07 UTC indicate an underestimation of the emissions, while positive errors outside the two explosive eruptions indicate an overestimation of the emissions. This diffusion effect reflects the typical challenge of solving ill–posed problems in reconstructing sharp spatial and temporal gradients. Nonetheless, the height and final time of the eruption are well analyzed by the ensemble mean on both days, which is basically a result of including no-volcanic ash observations.

The analyzed emission profile on 29 April 2010 shows the limits of the ESIAS-chem approach. While the volcanic ash

335 column mass loading have only low errors, the emission profile shows large deviations up to 60 unit% and more (Fig. 10c). The ensemble standard deviation of the emission profile (Fig. 10d) is lower than the relative error of the ensemble mean and ranges around 20 %. The results indicate that on 29 April 2010 the mixing of volcanic ash in the atmosphere is too effective,

which prohibits a proper estimate of volcanic ash emission profiles. However, the previous results show that even though the volcanic ash emission profile could not be properly estimated by the system on 29 April 2010, the vertical and horizontal

340   distribution of volcanic ash in the atmosphere is fairly represented by the ensemble mean.

The proper analysis of high volcanic ash concentrations in the atmosphere as well as their forecast accuracy are of great importance for air safety advisory services. Yet, only the ability of ESIAS-chem to provide reasonable estimates of vertically resolved volcanic ash forecasts and analysis is shown. Thus, the following analysis is dedicated to the accuracy of the ensemble prediction of volcanic ash using the 24 hour assimilation window experiment. Fig. 11a) compares the probability of volcanic

345   ash column mass loading exceeding $2\,\mathrm{gm}^{-2}$ on 16 April 2010, 00 UTC. Additionally, the nature run's volcanic ash column mass loading contours for 0.5, 1, and $2\,\mathrm{gm}^{-2}$ are overlaid by blue lines. On 15 April 2010, wind conditions are favorable for volcanic ash to disperse rapidly. Thus, the area containing high volcanic ash column mass loading covers only a small region above South-Sweden. The ensemble predicts a probability of more than $90\,\%$ for high volcanic ash column mass loading in
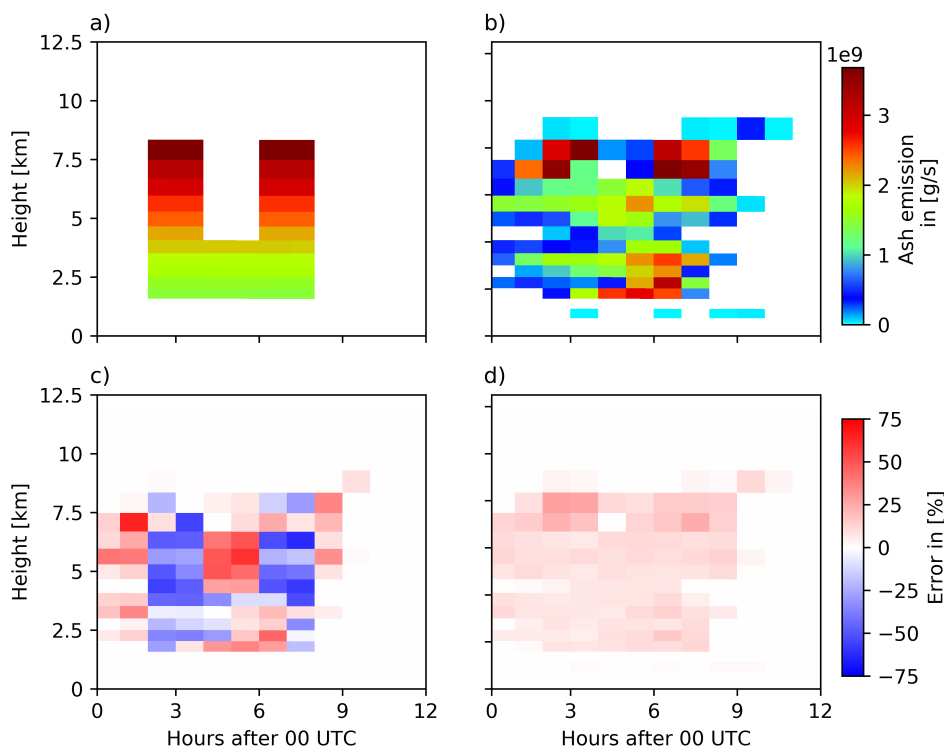
Figure 10. Comparison of the emission profiles of the nature run and ensemble mean for 29 April 2010. The figure shows (a) the nature run emission profile and (b) the ensemble mean emission profile. For comparison, (c) the relative error of the ensemble mean and (d) the relative ensemble standard deviation are illustrated.
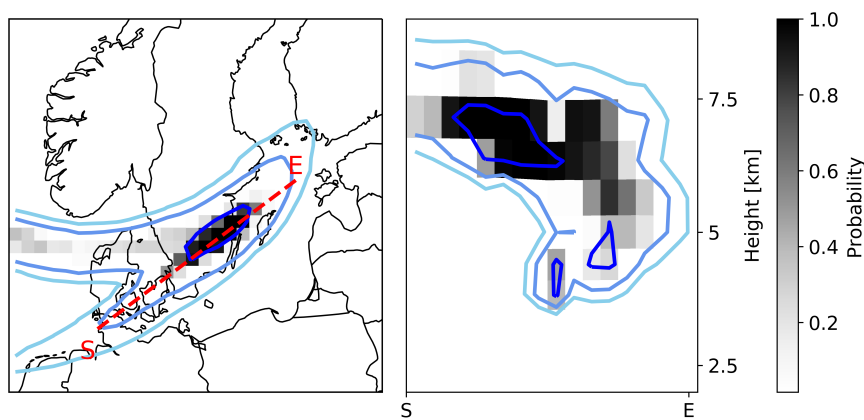
Figure 11. Probability maps on 16 April 2010, 00 UTC, from the 24 h assimilation window test case. a) Probability of the analysis ensemble for volcanic ash column mass loading exceeding 2 gm^{-2}. Contour lines of nature run volcanic ash column mass loading for 0.5, 1, and 2 mgm^{-2} are also given by blue lines. b) Probability of the analysis ensemble of volcanic ash concentration exceeding 500 $\mathrm{\mu gm}^{-3}$ along the red dashed line in a). Contour lines of nature run volcanic ash concentrations for 250, 350, and 500 $\mathrm{\mu gm}^{-3}$ are shown by blue lines.

this area. A small probability of about 20-30 % of volcanic ash column mass loading exceeding the threshold of 2 gm^{-2} is
350 also predicted above the North Sea, where nature run's volcanic ash column mass loading exceeds 1 gm^{-2}. Fig. 11b shows
the vertical cross-section along the red line in Fig. 11a, where the shading shows the probability of volcanic ash exceeding
500 $\mathrm{\mu gm}^{-3}$. Nature run's volcanic ash concentrations are displayed by isolines of 250, 350, and 500 $\mathrm{\mu gm}^{-3}$. As the dispersion
of volcanic ash leads to low volcanic ash concentrations on 16 April 2010, 00 UTC, the threshold of 500 $\mathrm{\mu gm}^{-3}$ for calculating
the exceedance probability was chosen instead of using the official threshold of 2 mgm^{-3} (Prata and Prata, 2012, and references
355 therein). The nature run's volcanic ash concentrations of more than 500 $\mathrm{\mu gm}^{-3}$ in about 7 km height are well represented by
the ensemble with high probability (> 90 %). Two other locations in this vertical cross-section show nature run's volcanic
ash concentrations above 500 $\mathrm{\mu gm}^{-3}$ in approx. 4 km height in the center of the vertical cross-section and in approx. 5 km
height northeast of the center (i. e. to the right in Fig. 11b). Even though the volcanic ash in 4 km height in the center of
the cross-section is covered from above by the elevated volcanic ash in 7 km height, the ensemble predicts a 50 % chance of
360 volcanic ash at 4 km height. This is remarkably, since only vertically integrated observations of volcanic ash are assimilated.
The volcanic ash northeast of the center of the vertical cross-section (i. e. to the right in Fig. 11b) is predicted by only 20-30 %
of the ensemble. The ensemble predicts this volcanic ash in this vertical column to be at a height of 6-7 km by a chance of
more than 70 %. This may be because of the lack of vertical wind shear that prevents the distinction of volcanic ash emitted at
different heights.
365 Fig. 12a shows the probability of volcanic ash column mass loading exceeding 2 gm^{-2} as predicted by the ensemble on
30 April 2010, 12 UTC, i. e. 36 hours after the simulation start and 12 hours after the end of the assimilation window. Isolines
of nature run's volcanic ash column mass loading for 0.5, 1, and 2 gm^{-2} are also given by blue lines. A vertical cross-section
of the probability of volcanic ash concentration exceeding 2 mgm^{-3} along the red line in Fig. 12a is shown in Fig. 12b. Even
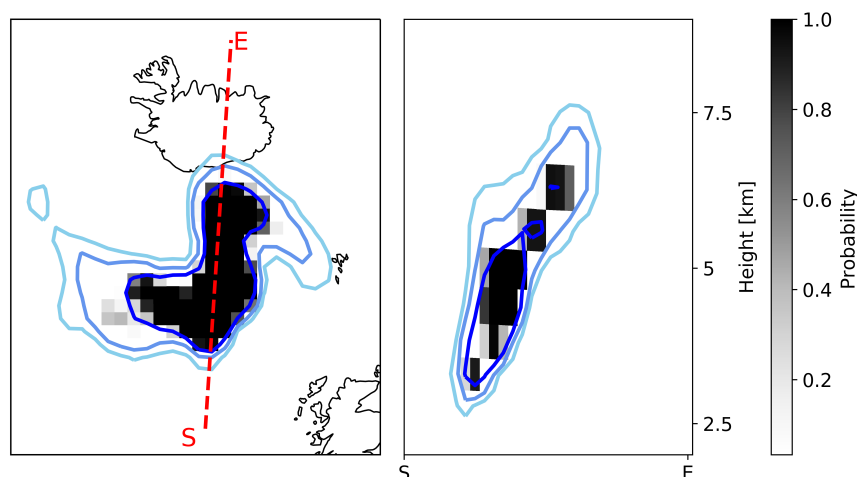
Figure 12. Probability map on 30 April 2010, 12 UTC, from the 24 h assimilation window test case. a) Probability of the analysis ensemble for volcanic ash column mass loading exceeding $2\ \mathrm{gm}^{-2}$. Contour lines of nature run volcanic ash column mass loading for 0.5, 1, and $2\ \mathrm{gm}^{-2}$ are also given by blue lines. b) Probability of the analysis ensemble of volcanic ash concentrations exceeding $2\ \mathrm{mgm}^{-3}$ along the red dashed line in a). Contour lines of nature run volcanic ash concentrations for 0.5, 1, and $2\ \mathrm{mgm}^{-3}$ are shown by blue lines.

though the emission profile on 29 April 2010 was not well analyzed, the ensemble predicts the high volcanic ash concentration
370 with a probability of more than 90 %. Thus, ESIAS-chem demonstrates to estimate the vertical distribution of volcanic ash in the atmosphere on both simulation days with a high accuracy.

4 Conclusions

In this study, a new method for estimating volcanic ash emissions and its uncertainty from column mass loading observations is developed. This new method is realized by the atmospheric chemical part of the Ensemble for Stochastic Integration of
375 Atmospheric Simulations (ESIAS-chem). On the one hand, the method comprises an ensemble-based particle smoother, which extends the assimilation window to include the latest observations available, taken for the estimation of the emission profile for the whole assimilation window. On the other hand, the discrete-grid ensemble Nelder-Mead method (DENM) is developed in order to efficiently achieve a posterior ensemble representation of the optimum of the cost function. The particle smoother approach enables to use the latest observations for the emission within the whole assimilation window.

380 The presented investigation acts as a best case scenario for probabilistic volcanic ash assessments. The analysis is idealized in different ways: Firstly, the uncertainties in meteorological fields, especially in winds, is neglected in the study. Secondly, the amount of observational data is exceptionally large, with observations of the full domain every 6 hours. The inclusion of observations of ash-free areas supports the systems ability to constraint the emissions to the correct times and heights. However, in a companion paper, ESIAS-chem is applied to real observations of volcanic ash. This study will also deal with the ability

385 of the system to remove volcanic ash emissions at false height and times. Even though direct observations of volcanic ash were used in this study, ESIAS-chem is extremely flexible in terms of observational data. By estimating the emission profile the system is able to use other kind of observations not directly related to volcanic ash in the atmosphere, such as samples of tephra fall out, if available.

  The flexibility of the system enables also to account for constraints on the emission profile. Those may result from radar or
390 web cam observations (e. g., Arason et al., 2011). It is noted that the vertical and temporal resolution of the emissions may be increased if it is suggested by information about the respective volcanic eruption. By the choice of an u-shaped emission profile, ESIAS-chem was challenged with highly variable volcanic ash emissions. By leaving the emission profile as unconstrained as possible, the system proves at least for strong wind conditions to estimate the emission profile even for this challenging situation.

395 The analysis showed that an assimilation window of 24 hours is sufficient in order to provide reliable forecasts of the vertically resolved volcanic ash distribution in the atmosphere. The system verifies to capture high volcanic ash concentrations in the correct height with a high probability. Although the system lacks to estimate the true emission profile sufficiently well for weak wind conditions, the analysis of the probability of volcanic ash showed that its vertical distribution in the atmosphere is accurately predicted.

400 Besides volcanic ash eruptions, ESIAS-chem is applicable to a variety of emission scenarios, especially unexpected emission events like forest fires and mineral dust events. Therefore, it provides a fast and efficient model for source term estimation including uncertainty representation. In principle, the method can be adapted to multi-source emission scenarios. The enhanced need for compute resources can partly be absorbed by a reduced resolution of the emission profile and will be in the focus of future work. Further, for the investigation of real volcanic eruptions, the uncertainties of meteorological variables, especially
405 winds, need to be represented. It is noted that ESIAS-chem is flexible in integrating other modules and is applicable to other atmospheric models as well.

Code availability. The analysis module used to calculate the volcanic ash emission estimate can be downloaded at http://doi.org/10.5281/zenodo.4736071 under a Creative Commons Attribution 4.0 International License.

Author contributions. PF designed the code extension necessary for this analysis. HE contributed mainly to the idea of ensemble estimation
410 of emission uncertainties. Main input regarding satellite observations and its uncertainty was given by ACL. All authors contributed equally to the manuscript.

Competing interests. The authors declare that they have no competing interests.

Acknowledgements. The authors gratefully acknowledge the Gauss Centre for Supercomputing e.V. (www.gauss-centre.eu) for funding this project by providing computing time through the John von Neumann Institute for Computing (NIC) on the GCS Supercomputer JUQUEEN
415 at Jülich Supercomputing Centre (JSC). The authors specially acknowledge Olaf Stein and Sebastian Lürs from JSC for their support of implementing the ensemble version of the EURAD-IM and improving its performance. This work is part of the Helmholtz program Earth System Knowledge Platform (ESKP) and was established in the Helmholtz Interdisciplinary Doctoral Training in Energy and Climate Research (HITEC) at Forschungszentrum Jülich and in the Graduate School of Geosciences (GSGS) at the University of Cologne.

References

420 Arason, P., Petersen, G. N., and Bjornsson, H.: Altitude estimates of the volcanic plume-top measured by C-band weather radar, pp. 9–17, PANGEA, in supplement to: Arason, P. et al. (2011): Observations of the altitude of the volcanic plume during the eruption of Eyjafjallajökull, April-May 2010. Earth System Science Data, 3(1), 9-17, https://doi.org/10.5194/essd-3-9-2011, 2011.

Bardintzeff, J.-M. and McBirney, A. R.: Volcanology, Jones & Bartlett Learning, 2000.

Bengtsson, T., Bickel, P., and Li, B.: Curse-of-dimensionality revisited: Collapse of the particle filter in very large scale systems, in: Prob-
425 ability and Statistics: Essays in Honor of David A. Freedman, edited by Nolan, D. and Speed, T., vol. 2 of *Collections*, pp. 316–334, Institute of Mathematical Statistics, Beachwood, Ohio, USA, https://doi.org/10.1214/193940307000000518, http://dx.doi.org/10.1214/193940307000000518, 2008.

Bickel, P., Li, B., and Bengtsson, T.: Sharp failure rates for the bootstrap particle filter in high dimensions, in: Pushing the limits of contemporary statistics: Contributions in honor of Jayanta K. Ghosh, vol. 3, pp. 318–329, Institute of Mathematical Statistics, 2008.

430 Bursik, M., Jones, M., Carn, S., Dean, K., Patra, A., Pavolonis, M., Pitman, E. B., Singh, T., Singla, P., Webley, P., Bjornsson, H., and Ripepe, M.: Estimation and propagation of volcanic source parameter uncertainty in an ash transport and dispersal model: Application to the Eyjafjallajökull plume of 14-16 April 2010, Bull Volc., 74, 2321–2338, https://doi.org/10.1007/s00445-012-0665-2, 2012.

Daley, R.: Atmospheric Data Analysis, Cambridge Univ. Press, 1991.

Dare, R. A., Smith, D. H., and Naughton, M. J.: Ensemble prediction of the dispersion of volcanic ash from the 13 February 2014 eruption
435 of Kelut, Indonesia, J. Appl. Meteor. Clim., 55, 61–78, 2016.

Denlinger, R. P., Pavolonis, M., and Sieglaff, J.: A robust method to forecast volcanic ash clouds, J. Geophys. Res., 117, 2012.

Eckhardt, S., Prata, A. J., Seibert, P., Stebel, K., and Stohl, A.: Estimation of the vertical profile of sulfure dioxide injection into the atmosphere by a volcanic eruption using satellite column meansurements and inverse transport modeling, Atmos. Chem. Phys., 8, 3881–3897, 2008.

440 Elbern, H., Strunk, A., Schmidt, H., and Talagrand, O.: Emission rate and chemical state estimation by 4-dimensional variational inversion, Atmos. Chem. Phys., 7, 1–59, 2007.

Folch, A., Costa, A., and Macedonio, G.: FPLUME-1.0: An integral volcanic plume model accounting for ash aggregation, Geosci. Model Dev., 9, 431–450, 2016.

Gao, F. and Han, L.: Implementing the Nelder-Mead simplex algorithm with adaptive parameters, Comput. Optim. Appl., 51, 259–277,
445 https://doi.org/10.1007/s10589-010-9329-3, 2012.

Gordon, N. J., Salmond, D. J., and Smith, A. F. M.: Novel approach to nonlinear/non-Gaussian Bayesian state estimation, in: IEE Proceedings-F (Radar and Signal Processing), vol. 140, pp. 107–113, 1993.

Houtekamer, P. L. and Mitchell, H. L.: Data assimilation using an ensemble Kalman filter technique, Month. Weath. Rev., 126, 796–811, 1998.

450 Jülich Supercomputing Centre: JUQUEEN: IBM Blue Gene/Q Supercomputer System at the Jülich Supercomputing Centre, Journal of large-scale research facilities, 1, https://doi.org/10.17815/jlsrf-1-18, http://dx.doi.org/10.17815/jlsrf-1-18, 2015.

Klein, K. and Neira, J.: Nelder-Mead simplex optimization routine for large-scale problems: A distributed memory implementation, Comput. Econ., 43, 447–461, 2014.

Kristiansen, N. I., Stohl, A., Prata, A. J., Bukowiecki, N., Dacre, H., Eckhardt, S., Henne, S., Hort, M. C., Johnson, B. T., Marenco, F., Neininger, B., Reitebuch, O., Seibert, P., Thomson, D. J., Webster, H. N., and Weinzierl, B.: Performance assessment of a volcanic ash transport model mini-ensemble used for inverse modeling of the 2010 Eyjafjallajökull eruption, J. Geophys. Res., 117, 2012.

Kristiansen, N. I., Prata, A. J., Stohl, A., and Carn, S. A.: Stratospheric volcanic ash emissions from the 13 February 2014 Kelut eruption, Geophys. Res. Lett., 42, 588–596, 2015.

Lagarias, J. C., Reeds, J. A., Wright, M. H., and Wright, P. E.: Convergence properties of the Nelder-Mead simplex method in low dimensions, SIAM J. Optim., 9, 112–147, 1998.

Lee, D. and Wiswall, M.: A parallel implementation of the simplex function minimization routine, Comput. Econ., 30, 171–187, https://doi.org/10.1007/s10614-007-9094-2, 2007.

Liu, J. S. and Chen, R.: Sequential Monte Carlo methods for dynamic systems, J. Americ. Stat. Assoc., 93, 1032–1044, 1998.

Lu, S., Lin, H. X., Heemink, A. W., Fu, G., and Segers, A. J.: Estimation of volcanic ash emissions using trajectory-based 4d-var data assimilation, Month. Weath. Rev., 144, 575–589, 2016.

Madankan, R., Pouget, S., Singla, P., Bursik, M., Dehn, J., Jones, M., Patra, A., Pavolonis, M., Pitman, E. B., Singh, T., and Webley, P.: Computation of probabilistic hazard maps and source parameter estimation for volcanic ash transport and dispersion, J. Comp. Phys., 271, 39–59, 2014.

Mastin, L. G., Guffanti, M., Servranckx, R., Webley, P., Barsotti, S., Dean, K., Durant, A., Ewert, J. W., Neri, A., Rose, W. I., Schneider, D., Siebert, L., Stunder, B., Swanson, G., Tupper, A., Volentik, A., and Waythomas, C. F.: A multidisciplinary effort to assign realistic source parameters to models of volcanic ash–cloud transport and dispersion during eruptions, J. Volc. Geotherm. Res., 186, 10–21, 2009.

McKinnon, K. I. M.: Convergence of the Nelder-Mead simplex method to a nonstationary point, SIAM J. Optim., 9, 148–158, 1998.

Nelder, J. A. and Mead, R.: A simplex method for function minimization, Comp. J., 7, 308–313, 1965.

Prata, A. J. and Prata, A. T.: Eyjafjallajökull volcanic ash concentrations determined using Spin Enhanced Visible and Infrared Imager measurements, J. Geophys. Res., 117, 2012.

Schmehl, K. J., Haupt, S. E., and Pavolonis, M. J.: A genetic algorithm variational approach to data assimilation and application to volcanic emissions, Pure Appl. Geophys., 169, 519–537, 2012.

Schmetz, J., Pili, P., Tjemkes, S., Just, D., Kerkmann, J., Rota, S., and Ratier, A.: An introduction to Meteosat Second Generation (MSG), Bull. Amer. Meteor. Soc., 83, 977–992, 2002.

Snyder, C., Bengtsson, T., Bickel, P., and Anderson, J.: Obstacles to high-dimensional particle filtering, Month. Weath. Rev., 136, 4629–4640, 2008.

Sparks, R. S. J., Bursik, M. I., Carey, S. N., Gilbert, J., Glaze, L. S., Sigurdsson, H., and Woods, A.: Volcanic plumes, John Wiley, Chichester, N. Y., USA, 1997.

Stefanescu, E. R., Patra, A. K., Bursik, M. I., Madankan, R., Pouget, S., jones, M., Singla, P., Singh, T., Pitman, E. B., Pavolonis, M., Morton, D., Webley, P., and Dehn, J.: Temporal, probabilistic mapping of ash clouds using wind field stochstic variability and uncertain eruption source parameters: Example of the 14 April 2010 Eyjafjallajökull eruption, J. Adv. Model. Earth Syst., 6, 1173–1184, 2014.

Stohl, A., Prata, A. J., Eckhardt, S., Clarisse, L., Durant, A., Henne, S., Kristiansen, N. I., Minikin, A., Schumann, U., Seibert, P., Stebel, K., Thomas, H. E., Thorsteinsson, T., Tørseth, K., and Weinzierl, B.: Determination of time- and height-resolved volcanic ash emissions and their use for quantitative ash dispersion modeling: the 2010 Eyjafjallajökull eruption, Atmos. Chem. Phys., 11, 4333–4351, 2011.

van Leeuwen, P. J.: Particle filtering in geophysical systems, Month. Weath. Rev., 137, 4089–4114, 2009.

Wilkins, K., Benedetti, A., Kristiansen, N., and Lange, A.: Chapter 13 - Applications of Satellite Observations of Volcanic Ash in Atmospheric Dispersion Modeling, in: Volcanic Ash, edited by Mackie, S., Cashman, K., Ricketts, H., Rust, A., and Watson, M., pp. 233 – 246, Elsevier, https://doi.org/https://doi.org/10.1016/B978-0-08-100405-0.00019-7, 2016a.

Wilkins, K. L., Mackie, S., Watson, I. M., Webster, H. N., Thomson, D. J., and Dacre, H. F.: Data insertion in volcanic ash cloud forecasting, Ann. Geophys., 57, 1–6, 2014.

Wilkins, K. L., Watson, I. M., Kristiansen, N. I., Webster, H. N., Thomson, D. J., Dacre, H. F., and Prata, A. J.: Using data insertion with the NAME model to simulate the 8 May 2010 Eyjafjallajökull volcanic ash cloud, J. Geophys. Res.: Atmos., 121, 306–323, 2016b.

Wilkins, K. L., Western, L. M., and Watson, I. M.: Simulating atmospheric transport of the 2011 Grímsvötn ash cloud using a data insertion update scheme, Atmos. Environ., 141, 48–59, 2016c.

Winker, D. M., Vaughan, M. A., Omar, A., Hu, Y., Powell, K. A., Liu, Z., Hunt, W. H., and Young, S. A.: Overview of the CALIPSO mission and CALIOP data processing algorithms, J. Atmos. Ocean. Technol., 26, 2310–2323, 2009.

Woodhouse, M. J., Hogg, A. J., Phillips, J. C., and Sparks, R. S. J.: Interaction between volcanic plumes and wind during the 2010 Eyjafjallajökull eruption, Iceland, J. Geophys. Res.: Sol. Ea., 118, 92–109, 2013.

Zidikheri, M. J., Potts, R. J., and Lucas, C.: A probabilistic inverse method for volcanic ash dispersion modelling, in: Proceedings of the 17th Biennial Computational Techniques and Applications Conference, CTAC-2014, edited by Sharples, J. and Bunder, J., vol. 56, pp. C194–C209, 2016.

Zidikheri, M. J., Lucas, C., and Potts, R. J.: Toward quantitative forecasts of volcanic ash dispersial: Using satellite retrievals for optimal estimation of source terms, J. Geophys. Res.: Atmos., 122, 8187–8206, 2017a.

Zidikheri, M. J., Lucas, C., and Potts, R. J.: Estimation of optimal dispersion model source parameters using satellite detections of volcanic ash, J. Geophys. Res.: Atmos., 122, 8207–8232, 2017b.